CHALMERS

Diffusion of large molecules in conifer bordered pits

Master of Science thesis in the master degree program Innovative and Sustainable Chemical Engineering

ADAM THERNING

Diffusion of large molecules in conifer bordered pits

Master of Science thesis in the master degree program Innovative and Sustainable Chemical Engineering

ADAM THERNING

Abstract

Bordered pits connect adjacent tracheid cells in softwoods and enable water transport between them. The pits are interruptions in the cell wall, consisting of a permeable margo with a centered impermeable torus and the cell wall overarching the margo and part of the torus.

Knowledge of how large molecules (such as hemicelluloses and enzymes) are transported through pits is important for effectively extracting biopolymers from wood. Biopolymers can be used to produce renewable products, e.g. bioplastics, which can replace fossil fuel based materials.

The main transport mechanism for large dissolved molecules through bordered pits is diffusion. This work aims to find effective diffusion coefficients for large molecules through a pit and to determine the pit component's individual contribution to the diffusive resistance.

To achieve this, three models of a bordered pit was developed and the lattice Boltzmann method was used to simulate diffusion through these models. Molecular weights between 1 and 40 kDa were examined, since this is the molecular weights of interest during extraction.

It was found that the effective diffusion coefficient is 16.9 times smaller than the free diffusion coefficient. The borders, torus and margo constitutes 98.8, 1.1 and 0.1 % of the total resistance to diffusion respectively. To increase the diffusive mass transfer rate through pits it is therefore necessary to partially or entirely remove the borders.

Keywords: lattice Boltzmann method, simulation, diffusion, bordered pit, conifer, softwood

Acknowledgments

Contents

1   Introduction

Global warming is a major contemporary environmental concern. It is likely that the reason is increased atmospheric concentration of greenhouse gases, largely due to human use of fossil fuels. [1] This has strengthened the incentive to consider more sustainable raw materials for production of chemicals and value-added products. A promising alternative is lignocellulosic materials [2].

Lignocellulosic biomass is mainly comprised of complex networks of cellulose, hemicellulose and lignin. In a material-driven biorefinery, extraction of these components as long polymers is desired, but the entangled structure aggravates the separation. The extraction can be enhanced by adding enzymes to cut crucial bonds in the network. For the large enzymes to effectively reach the reaction sites the wood structure has to be loosened up. [3] Mild steam explosion is a pretreatment method which increases the cross-sectional area available for diffusion by introducing cracks in the wood structure [4].

For biorefinery products to be competitive with the fossil alternatives the cost efficiency has to be improved. The pretreatment and enzyme addition are expensive [5] and knowledge of the mechanisms occurring in those production steps are important for designing efficient overall processes.

In softwoods, most of the biopolymers and lignin are found in tracheid cell walls [6]. Tracheids transport water and provides stability and strength to the tree [7]. Adjacent tracheids are connected by bordered pits, as shown in fig 1. The pits are interruptions in the cell wall, consisting of a permeable margo with a centered impermeable torus and the cell wall overarching the margo and part of the torus (fig 3). [8]

Behr et al [9] used an experimental approach to study diffusion of sodium chloride and naphthalene through wood. Diffusion of water vapor through pits was modelled using the finite difference method by Wadsö [10]. Valli et al [11] used the lattice Boltzmann method to simulate water flow through bordered pits, but the membrane was modelled as a porous medium. Schulte [8] and Schulte et al [12] developed detailed models of bordered pits and utilized computational fluid dynamics to study water flow through them.

The diffusive behavior of large molecules in pits has not been investigated, but is an important field of study in understanding how biopolymers and enzymes move through the wood structure. This work aims to find effective diffusion coefficients through conifer bordered pits for biopolymers and enzymes and to determine the pit component's individual contribution to the diffusion resistance. Molecular weights between 1 and 40 kDa were examined, since this is the molecular weights of interest during extraction [13].

2 Background

In this section a brief introduction to the structure of conifers is given, as well as an in-depth description of bordered pits. Thereafter, the mechanism for diffusion of mass and the lattice Boltzmann method for simulating diffusion is described.

2.1 Structure of conifers

Softwoods are comprised of longitudinal and radial tracheid and parenchyma cells. Tracheids transport water and provide stability and strength to the tree. Parenchyma cells produce extractives, stores starch and surrounds resin canals. [7] More than 90 % of the total volume is longitudinal tracheids. Their length is commonly between 1.2 and 7.5 mm and the diameter is approximately 1 % of the length. [6] Earlywood tracheids are formed during the first part of the growth season and have large cell lumens and thin walls compared to tracheids in latewood. [14] Earlywood constitutes 40 - 80 % of conifer width and accounts for up to 90 % of the water flow path [15]. Figure 1 shows longitudinal tracheids in earlywood and latewood in Norway spruce (*Picea abies*).
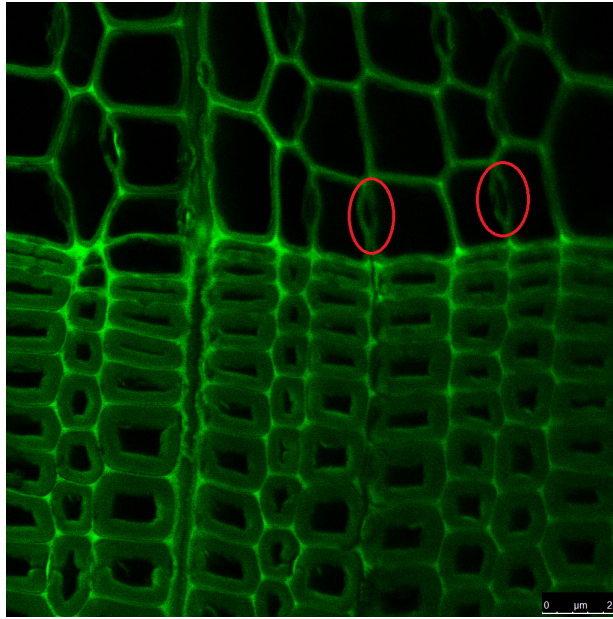
Figure 1: A confocal fluorescent scanning laser microscopy (CFSLM) image of longitudinal tracheids in earlywood and latewood in Norway spruce (*Picea abies*). Two bordered pits are circled. Courtesy of P. Kvist.

Neighboring tracheids are connected by bordered pits, as shown in fig 1. The pits are interruptions in the cell wall, consisting of a permeable margo with a centered impermeable torus and the cell wall overarching the margo and part of the torus. Figure 3 shows the general structure of a bordered pit. The margo and torus (together called membrane) in a bordered pit in Grand fir (*Abies grandis*) are shown in figure 2.

Figure 2: Margo and torus in a bordered pit. Based on a SEM image of an earlywood bordered pit in Grand fir (*Abies grandis*) by Petty [16].

Figure 3: Structure and nomenclature of a bordered pit.

Pits enable transport of water between tracheids. Air embolisms are inhibited to spread since their presence aspirates the pits by displacing the torus to the borders. The aspiration impedes water transport between adjacent tracheids. [8]
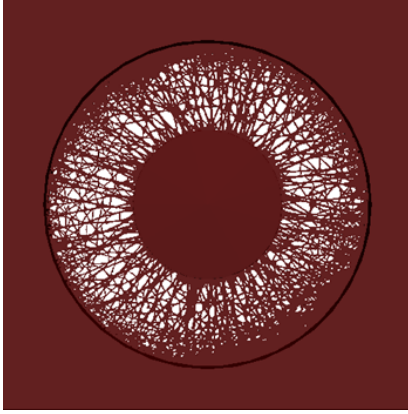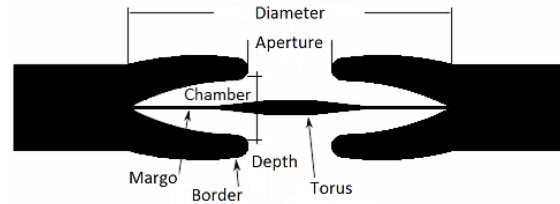
Hacke et al [17] studied bordered pits in 16 different conifers and found the diameter to vary between 6 and 20 μm. Siau [6] state pit diameters to commonly range from 6 to 30 μm and earlywood pits to be larger and have a less compact margo than latewood pits. Pit dimensions and margo structure are also dependent on tree species and growth conditions [8, 18], but variations are large even within the same tree [12, 19, 20].

The diameter of the aperture is about 50 % of the torus diameter, which usually is 33 to 50 % of the pit diameter [6]. Reported values for torus thickness vary between 0.3 and 1.0 μm [6, 21]. The margo is approximately 0.025 to 0.5 μm thick [6, 8]. Schulte [8] and Schulte et al [12] state values for pit depth between 2.28 and 4.57 μm, and that is supported by Petty [16] and Wadsö [10].

The margo strands consist of cellulose, and the torus and cell wall are comprised of cellulose, hemicellulose and lignin [6]. Cellulose is the most abundant component in softwood, as it constitutes approximately 42 wt-%. Hemicellulose and lignin make up about 27 and 28 wt-% respectively. Extractives and inorganic compounds are mainly found in the cell lumen and accounts for the remaining 3 wt-%. [22]

Cellulose is a polysaccharide made up by thousands of glucose monosaccharides. Up to 40 cellulose polymers are arranged into crystalline microfibrils. The microfibrils are thin and long and provide tensile strength to the tree. Lignin is an irregularly structured polymer comprised of hundreds of aromatic phenylpropane units. Lignin inhibits both deformation of microfibrils and biodegradation. Hemicellulose is an umbrella term for several polysaccharides. They have a random structure [23], are smaller than cellulose and consist of glucose but also other monomers, such as xylose, mannose and arabinose. Glucomannan and arabinoglucoronxylan are the most abundant hemicelluloses in softwoods. The function of hemicelluloses is

ambiguous, but most probable is that they tie lignin and cellulose together. [22]

2.2 Diffusion of mass

Diffusion is a process where random movement of individual molecules occur concurrent with a net movement of molecules from a zone of high concentration to a zone of low concentration. A mathematical description of diffusion for an isotropic system with constant temperature and pressure is given in rectangular coordinates by eq 1.

$$\frac{\partial C_1}{\partial t} = D_{12} \left(\frac{\partial^2 C_1}{\partial x^2} + \frac{\partial^2 C_1}{\partial y^2} + \frac{\partial^2 C_1}{\partial z^2} \right) \tag{1}$$

where C_1 is the concentration of specie 1, D_{12} is the diffusion coefficient of specie 1 in specie 2 and t is the time. The diffusion is assumed to occur in three dimensions and x, y and z represent the directional axes. [24–26] The diffusive flux of specie 1, J_1, is described by Fick's first law (eq 2) [26].

$$J_1 = -D_{12} \nabla C_1 \tag{2}$$

The diffusion coefficient is generally high for gases, low for liquids and very low for solids. It is dependent on temperature, pressure and concentration, but also on size and form of the diffusing specie. There are numerous ways of estimating this coefficient, both experimentally and theoretically. The Stokes-Einstein equation (eq 3) determines diffusion coefficients of large rigid spherical molecules in dilute liquids with a precision of 20 %. [25]

$$D_{12} = \frac{k_B T}{6\pi \mu R_0} \tag{3}$$

k_B is the Boltzmann's constant, T is the temperature, μ is the viscosity of the solvent and R_0 is the radius of the diffusing molecule. [26] Dissolved enzymes commonly forms spherical globules [27] which enables the use of eq 3. If the assumption of sphericity is not valid the radius in eq 3 can be replaced with an equivalent radius. This is necessary for dissolved polymers, since they are not spherical but more or less stretched out. [25]

If the solution is constrained by a complex geometry the rate of diffusion is decreased. The geometry act as an obstacle, forcing the diffusing specie to travel longer distance. To take this into account the free diffusion coefficient is modified into an effective diffusion coefficient. [25] There are several ways to do this, but commonly it includes scaling with the tortuosity and porosity. The tortuosity is defined as the ratio of the length of the path for hindered diffusion to the length of the path for free diffusion. [28]

2.3 Lattice Boltzmann method for diffusion

The lattice Boltzmann method is an algorithm applicable to simulating diffusion. It solves the diffusion equation (eq 1) by modelling fluid molecules as rigid particles,

and a statistical approach is used to avoid individual tracing of the particles. [29] This section describes the lattice Boltzmann method and explain why it is the preferable method for simulating diffusion in complex geometries.

2.3.1 The Boltzmann transport equation

The Boltzmann transport equation (eq 4) is the foundation of the lattice Boltzmann method.

$$\frac{\partial f}{\partial t} + \boldsymbol{c}\nabla f + \frac{\boldsymbol{F}}{m}\frac{\partial f}{\partial \boldsymbol{c}} = \Omega \tag{4}$$

where f is the velocity distribution function for molecules confined by $\boldsymbol{r}$ and $\boldsymbol{r} + \partial\boldsymbol{r}$ at time t. $\boldsymbol{c}$ is the particle velocity, $\boldsymbol{F}$ is an external force (e.g. gravity) acting on the particles, m is the molecular mass and Ω is the collision operator. [29]

Particles influenced by an external force are accelerated or decelerated. If the force and the distribution function is known at time t and the particles do not collide, it is possible to find the distribution function at time $t + dt$. This process is called streaming and is described by the left side of eq 4. The right side of eq 4 incorporate the collisional effect into the model by accounting for the change in the distribution function when particles streaming towards a certain position collide and end up somewhere else. [30]

The collision operator is dependent on the distribution function in a complex way, which makes the Boltzmann transport equation difficult to solve. By replacing it with the Bhatnagar-Gross-Krook approximation (eq 5) the computational cost is reduced. [29]

$$\Omega = \frac{1}{\tau}(f^{eq} - f) \tag{5}$$

The main idea behind the approximation is that collisions occur because the distribution function deviates from equilibrium. f^{eq} is the local equilibrium distribution function towards which the distribution function is relaxed. The relaxation rate is determined by the relaxation factor τ. [31] There are schemes utilizing two or more relaxation factors (two- and multi-relaxation-time schemes), by splitting the distribution function into two or more parts [32]. Higher order schemes have higher accuracy and stability than the simpler Bhatnagar-Gross-Krook approximation. [29]

All parameters are dimensionless and the dimensionless domain is discretized by dividing it into equal sized lattices [33]. Particles are allowed to occupy a number of points at the lattice surface and interior. For 3D simulations the D3Q19 setup is commonly used. It assigns 19 points to each lattice, as visualized by fig 4. [29]
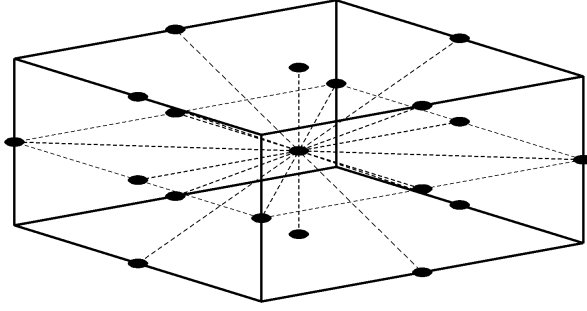
Figure 4: A lattice and the computational points in a D3Q19 setup.

The discrete Boltzmann transport equation with the Bhatnagar-Gross-Krook approximation is shown in eq 6.

$$f_i(\boldsymbol{r} + c_i\Delta t, t + \Delta t) - f_i(\boldsymbol{r}, t) + \frac{\Delta t}{N\boldsymbol{c}^2}c_iF_i(\boldsymbol{r}, t) = \frac{\Delta t}{\tau}(f_i^{eq}(\boldsymbol{r}, t) - f_i(\boldsymbol{r}, t)) \quad (6)$$

where subscript i ranges from 1 to 19, denoting each of the lattice points. N is a constant depending on the lattice pattern and Δt is the time step [34].

Particle collisions are assumed to only occur at the lattice sites, while streaming moves particles between them [29]. Therefore, the solving procedure of eq 6 is divided into two steps: first the right side is calculated to account for collisions, after which the left hand side is computed to account for streaming. [35]

The main difference in solving eq 6 for various problems lays in the equilibrium distribution function. For diffusive problems the equilibrium distribution function is given by eq 7.

$$f_i^{eq} = \Phi w_i \quad (7)$$

where Φ is the concentration and w_i is the weighting factor in the i direction. Over a computational lattice site the weighting factors sum to one and the equilibrium distribution functions sum to the dependent variable. [29]

2.3.2   Complex geometries

The wall boundary conditions are implemented by allowing particles at the lattice nodes located closest to the solid-fluid interface only stream to sites inside the fluid domain and not to sites in the solid [35,36]. This is a simple and cost efficient method of implementing the wall boundary conditions and gives the lattice Boltzmann an advantage over traditional computational fluid dynamics methods for simulation of diffusion in complex geometries [34,37].

3 Methodology

This section describes the bordered pit models used in the simulations and how biopolymers and enzymes were modeled using model molecules. The simulation settings and resolutions are presented, as well as how the effective diffusion coefficient was obtained and how the resistances of the individual pit components were determined. A theoretical expression for the effective diffusion coefficient through a pit is used to validate the simulation results. The derivation of this expression and the validation procedure are also described in this section.

3.1 Models of the bordered pit

The membrane structure was based on a scanning electron microscope (SEM) image of an earlywood bordered pit in Grand fir (*Abies grandis*) by Petty [16]. The SEM image was imported into Inkscape 0.91, a graphics editor. The trace bitmap command was used to vectorize the image based on the shade of the pixels. The vectorized two-dimensional membrane was imported into AutoCAD 2016, where it was extruded to three dimensions. AutoCAD was further used to create rest of the pit and a hollow square box surrounding it. Average pit dimensions were chosen based on literature values [6, 8, 10, 12, 16, 17, 21].

Three pit models were developed - representing an entire pit, a pit without margo and a pit without both margo and torus (tab 1).

Table 1: Components accounted for in each model.

Model	Included components
A	borders, torus, margo
B	borders, torus
C	borders

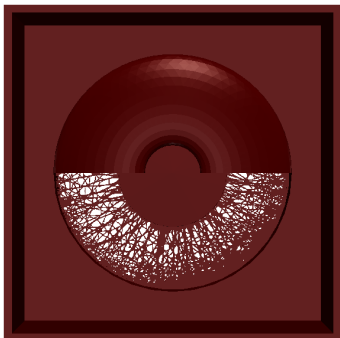Model A, B and C are visualized in fig 5, 6 and 7.

Figure 5: Model A. The borders are partially removed for illustrative purpose.
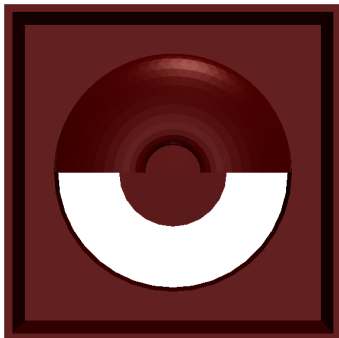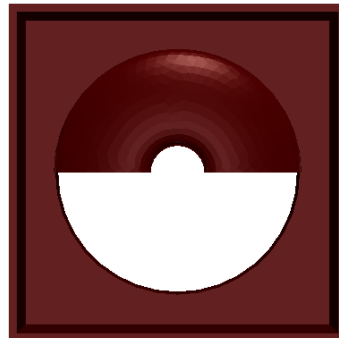
Figure 6: Model B.

Figure 7: Model C.

Table 2 shows the dimensions of the bordered pit. The nomenclature is same as in fig 3.

Table 2: Dimensions of the bordered pit.

Pit component dimension	Size [μm]
Margo thickness	0.05
Torus thickness (center)	0.50
Torus diameter	7.45
Pit diameter	16.10
Aperture diameter	3.70
Aperture depth	0.63
Pit depth	4.00

The simulation box dimensions are shown in tab 3, where z is the depth of the box and x and y are the cross-sectional components.

Table 3: Dimensions of the simulation box.

Box dimension	Length [μm]
x	12.00
z	20.00
y	20.00

3.2   Model molecules

The polysaccharide dextran was used as model molecule for the biopolymers, since free diffusion coefficients and equivalent radiuses are not available for them. Dextran and the biopolymers are both comprised of long chains of sugar monomers and the diffusive behavior of the two polymers is therefore expected to be similar. Arrio-Dupont et al [38] has determined free diffusion coefficients of dextran of various sizes in water (fig 8).
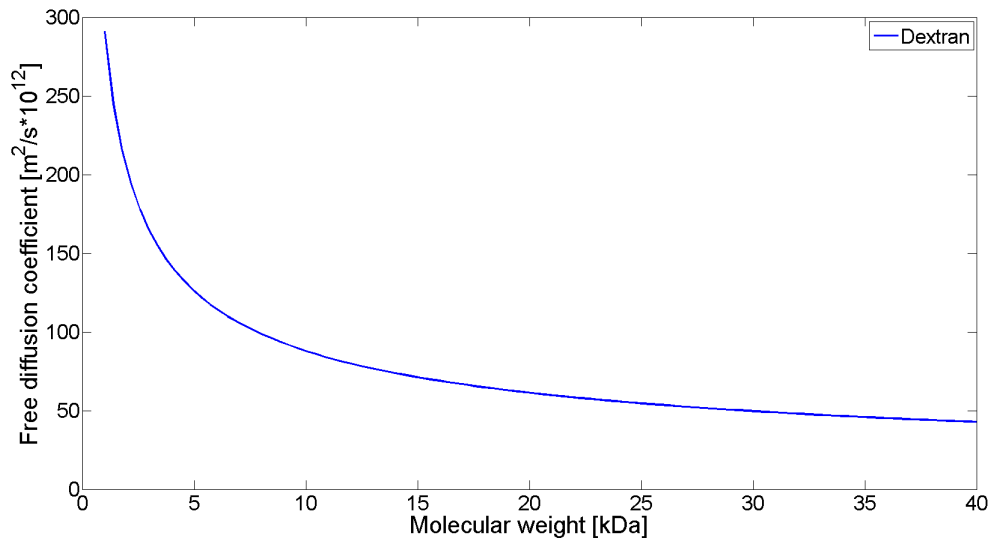

Figure 8: Free diffusion coefficients of dextran in water. [38]

The model enzyme is assumed to be spherical, which enables the use of eq 3 to calculate the free diffusivity and eq 8 to compute the radius required in eq 3.

8

$$R_0 = 0.066 M^{1/3} \tag{8}$$

where M is the enzyme weight in Dalton and R_0 is the radius in nanometer [27]. Figure 9 shows the free diffusion coefficient of the model enzyme in water for molecular weights between 1 and 40 kDa.
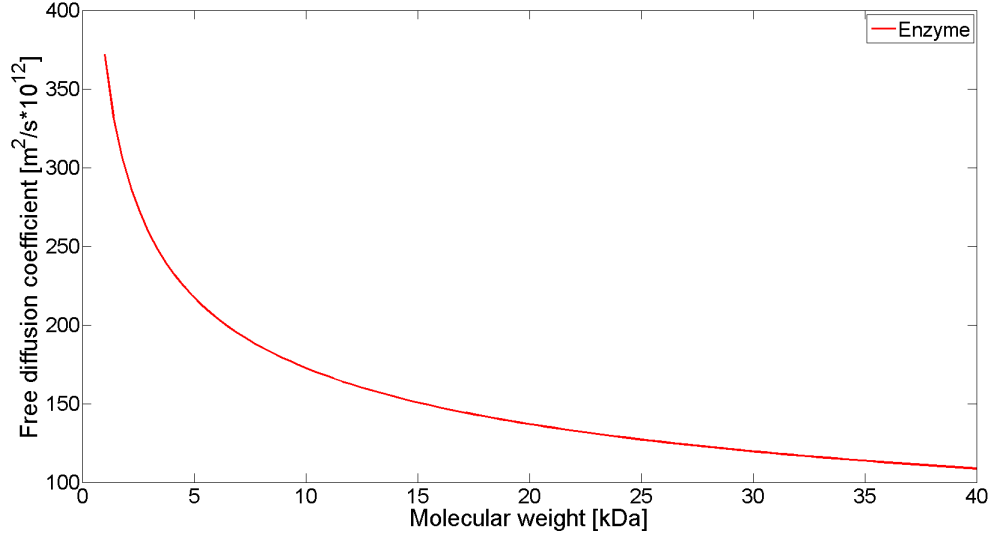

Figure 9: Free diffusion coefficients of the model enzyme in water.

The model molecules are assumed not to get stuck in the margo. This is confirmed by comparing the average radius of 0.12 μm for the margo pores in Grand fir (*Abies grandis*), reported by Petty [16], with the equivalent radius of a 40 kDa dextran molecule (calculated from eq 3, with the free diffusion coefficient from fig 8) and the radius of a 40 kDa enzyme (computed from eq 8), as shown in eq 9a and 9b.

$$\frac{r_{pore}}{R_{0,dextran}} = 19.5 \tag{9a}$$

$$\frac{r_{pore}}{R_{0,enzyme}} = 53.2 \tag{9b}$$

Since the ratios in eq 9a and 9b are much larger than 1, the pit membrane pores are significantly larger than the largest polymer and enzyme used in this work. The assumption is therefore valid.

3.3 Simulations

The pit models in fig 5, 6 and 7 were imported into Gesualdo 1.3.2 - a software for lattice Boltzmann simulations. The effective diffusion coefficient was computed by first solving eq 1 with the free diffusion coefficient (from fig 8 and 9) to steady state and thereafter solving eq 2 for the effective diffusion coefficient. This section describes the simulation settings and resolution.

3.3.1 Settings

To initiate the simulations a dimensionless concentration difference of the diffusing specie was specified. The concentration in the inlet and outlet was set to 1.05 and 1.00 respectively and the initial concentration profile was linear between the inlet and outlet concentration.

Cell walls, borders, margo strands and the torus were treated as impenetrable walls. The simulations were carried out with a D3Q19 lattice set-up and a two-relaxation-time scheme. It was assumed that no external force affects the system and that the solution is dilute so the diffusing molecules do not interact with each other.

3.3.2 Resolution

The simulations were carried out with six different resolutions - labelled S_1, S_2 and so on. Table 4 shows the number of lattices in the entire simulation box and in the x, y and z directions for each of the six cases.

Table 4: Number of lattices in the z, x and y directions and in entire simulation box.

Resolution	Number of lattices			
	x	z	y	total
S_1	286	500	500	$71.50 \cdot 10^6$
S_2	257	450	450	$52.04 \cdot 10^6$
S_3	229	400	400	$36.64 \cdot 10^6$
S_4	200	350	350	$24.50 \cdot 10^6$
S_5	172	300	300	$15.48 \cdot 10^6$
S_6	143	250	250	$8.94 \cdot 10^6$

By dividing the simulation box dimensions (tab 3) with the number of lattices in each direction (tab 4) the lattice size is obtained (tab 5).

Table 5: Dimensions of the lattices.

Resolution	Lattice size			
	x [µm]	z [µm]	y [µm]	volume [$µm^3 \cdot 10^4$]
S_1	0.042	0.040	0.040	0.67
S_2	0.047	0.044	0.044	0.92
S_3	0.052	0.050	0.050	1.31
S_4	0.060	0.057	0.057	1.96
S_5	0.070	0.067	0.067	3.10
S_6	0.084	0.080	0.080	5.37

The results in section 4 were obtained with the S1 resolution, while S2 - S6 were used in section 4.3.4 to investigate the grid dependence.

3.4 Resistance to diffusion

The pit component's individual contribution to the resistance to diffusion was computed by first relating the effective diffusion coefficient to the free diffusion coefficient for each model i (A, B or C), as shown in eq 10.

$$x_i = 1 - \frac{D_{eff,i}}{D_{12}} \tag{10}$$

where x_i is the normalized decrease of the free diffusion coefficient due to the obstacles imposed by model i. The part of the decrease accredited the borders are calculated by relating the normalized decrease of the model containing only the borders to the normalized decrease of the full pit model (eq 11).

$$R_{borders} = \frac{x_C}{x_A} \tag{11}$$

The only difference between model B and C is the presence of a torus in B but not in C. The torus resistance is therefore obtained as in eq 12.

$$R_{torus} = \frac{x_B - x_C}{x_A} \tag{12}$$

The margo resistance is calculated according to eq 13.

$$R_{margo} = \frac{x_A - x_B}{x_A} \tag{13}$$

3.5 Theoretical model

In this section a theoretical expression for the effective diffusion coefficient through model A (fig 5) is derived and the data used when calculating the effective diffusion coefficient with this model is reported.

3.5.1 Derivation

By integrating eq 2 along the x direction - assuming diffusion in one direction only - and multiplying both sides with the cross-sectional area available for diffusion, an expression for the diffusive molar flow is obtained (eq 14).

$$n_1 = -D_{12}A\frac{\Delta C_i}{\Delta x} \tag{14}$$

where n_1 is the molar flow of specie 1 and A is the cross-sectional area available for diffusion. ΔC_1 is the concentration difference of 1 and Δx is the distance of diffusion.

Equation 14 assumes free diffusion but by introducing an effective diffusion coefficient it can be applied to an entire pit (eq 15).

$$n_1 = -D_{eff,t}\bar{A}\frac{C_{in} - C_{out}}{\Delta x} \tag{15}$$

The cross-sectional area for diffusion in eq 15 is taken as a weighted mean area for the entire simulation box, where the area available for diffusion in each part of the box (aperture, chamber, membrane, box lumen) is weighted with the ratio of the length of that part to the total box length, as shown in eq 16.

$$\bar{A} = 2A_a\frac{\Delta x_a}{\Delta x} + 2A_c\frac{\Delta x_c}{\Delta x_{pit}} + A_m\frac{\Delta x_m}{\Delta x} + 2A_l\frac{\Delta x_l}{\Delta x} \tag{16}$$

11

The molar flow through each part of the pit is identical. By using eq 14 for each of the components the molar flow can be expressed as in eq 17a - 17g.

$$n_1 = -D_{12}A_a\frac{C_{0a_1} - C_{a_1}}{\Delta x_a} \tag{17a}$$

$$n_1 = -D_{12}A_a\frac{C_{0a_2} - C_{a_2}}{\Delta x_a} \tag{17b}$$

$$n_1 = -D_{12}A_c\frac{C_{0c_1} - C_{c_1}}{\Delta x_c} \tag{17c}$$

$$n_1 = -D_{12}A_c\frac{C_{0c_2} - C_{c_2}}{\Delta x_c} \tag{17d}$$

$$n_1 = -D_{12}A_l\frac{C_{0l_1} - C_{l_1}}{\Delta x_l} \tag{17e}$$

$$n_1 = -D_{12}A_l\frac{C_{0l_2} - C_{l_2}}{\Delta x_l} \tag{17f}$$

$$n_1 = -D_{12}A_m\frac{C_{0m} - C_m}{\Delta x_m} \tag{17g}$$

Subscript a_1 and a_2 denotes the first and second aperture, c_1 and c_2 the chambers, l_1 and l_2 the box lumens and m the membrane.

An expression for the concentration difference over the apertures, chambers, box lumens and membrane is obtained by rearranging eq 17a - 17g into eq 18a - 18g.

$$C_{0a_1} - C_{a_1} = \frac{n_1\Delta x_a}{-D_{12}A_a} \tag{18a}$$

$$C_{0a_2} - C_{a_2} = \frac{n_1\Delta x_a}{-D_{12}A_a} \tag{18b}$$

$$C_{0c_1} - C_{c_1} = \frac{n_1\Delta x_c}{-D_{12}A_c} \tag{18c}$$

$$C_{0c_2} - C_{c_2} = \frac{n_1\Delta x_c}{-D_{12}A_c} \tag{18d}$$

$$C_{0l_1} - C_{l_1} = \frac{n_1\Delta x_l}{-D_{12}A_l} \tag{18e}$$

$$C_{0l_2} - C_{l_2} = \frac{n_1\Delta x_l}{-D_{12}A_l} \tag{18f}$$

$$C_{0m} - C_m = \frac{n_1\Delta x_m}{-D_{12}A_m} \tag{18g}$$

The concentration difference over the entire pit is obtained by rearranging eq 15 into eq 19.

$$C_{in} - C_{out} = -\frac{n_1\Delta x}{D_{eff,t}\bar{A}} \tag{19}$$

The concentration difference in eq 19 can be expressed by adding the concentration differences for each pit part in eq 18a - 18g, as shown in eq 20 and 21a - 21h.

$$
\begin{aligned}
C_{in} - C_{out} = (C_{0l_1} - C_{l_1}) + (C_{0a_1} - C_{a_1}) + (C_{0c_1} - C_{c_1}) + \\
(C_{0m} - C_m) + (C_{0c_2} - C_{c_2}) + (C_{0a_2} - C_{a_2}) + (C_{0l_2} - C_{l_2})
\end{aligned}
\tag{20}
$$

since

$$C_{in} = C_{0l_1} \tag{21a}$$
$$C_{l_1} = C_{0a_1} \tag{21b}$$
$$C_{a_1} = C_{0c_1} \tag{21c}$$
$$C_{c_1} = C_{0m} \tag{21d}$$
$$C_m = C_{0c_2} \tag{21e}$$
$$C_{c_2} = C_{0a_2} \tag{21f}$$
$$C_{a_2} = C_{0l_2} \tag{21g}$$
$$C_{l_2} = C_{out} \tag{21h}$$

By using eq 20 and the right hand side of eq 18a - 18g the concentration difference over the entire pit can be expressed as in eq 22.

$$
C_{in} - C_{out} = -\frac{n_1}{D_{12}} \left(2\frac{\Delta x_a}{A_a} + 2\frac{\Delta x_c}{A_c} + \frac{\Delta x_m}{A_m} + 2\frac{\Delta x_l}{A_l} \right)
\tag{22}
$$

Combining eq 19 and 22 and solving for the effective diffusion coefficient gives a theoretical expression for the effective diffusion coefficient (eq 23).

$$
D_{eff,t} = \frac{D_{12}\Delta x}{\bar{A} \left(2\frac{\Delta x_a}{A_a} + 2\frac{\Delta x_c}{A_c} + \frac{\Delta x_m}{A_m} + 2\frac{\Delta x_l}{A_l} \right)}
\tag{23}
$$

Equation 23 assumes the torus and margo are of equal thickness and does not take the complex structure of the margo into account.

3.5.2 Data

Table 6 and 7 shows the data used in calculating the theoretical effective diffusion coefficient in eq 23. The dimensions are same as in the pit model used in the simulations (tab 2 and 3). The membrane area is obtained from the model in AutoCAD, by isolating the voids and calculating their area. The chamber area is taken as the average of the aperture area and the area of a circle with the same diameter as the membrane.

Table 6: Lengths used in the theoretical model.

Dimension	Length [μm]
Δx_a	0.63
Δx_l	3.37
Δx_c	1.98
Δx_m	0.05
Δx	12.00

Table 7: Areas used in the theoretical model.

Dimension	Area [μm²]
A_a	10.75
A_l	400.00
A_c	107.14
A_m	40.49
$\bar{A}$	261.32

3.6 Validation of results

This section describes how the theoretical model derived in section 3.5 was used for validation of the simulation results.

3.6.1 Effective diffusion coefficient

The effective diffusion coefficient obtained from the simulations was compared with the theoretical effective diffusion coefficient according to eq 24.

$$\frac{D_{eff,t}}{D_{eff}} \tag{24}$$

This ratio should be larger than 1 since the theoretical expression only consider the change in cross-sectional area available for diffusion across the pit and not the rapid geometrical changes between the pit components, the net-like structure of the margo or the blocking effect of the torus. A ratio larger than 10 implies a theoretical effective diffusion coefficient an order of magnitude larger than the effective diffusion coefficient obtained from the simulations. Such a large difference would be difficult to justify.

3.6.2 Resistances to diffusion

The part of the total theoretical resistance ascribed the membrane is computed according to eq 25.

$$R_{membrane,t} = \frac{\Delta x_m / A_m}{2\frac{\Delta x_a}{A_a} + 2\frac{\Delta x_c}{A_c} + \frac{\Delta x_m}{A_m} + 2\frac{\Delta x_l}{A_l}} \tag{25}$$

and is compared with the membrane resistance from the simulations (eq 12 and 13), as shown in eq 26.

$$\frac{R_{margo} + R_{torus}}{R_{membrane,t}} = \frac{R_{membrane}}{R_{membrane,t}} \tag{26}$$

The contribution of the borders (eq 27) is obtained by adding the contribution of the apertures, chambers and box lumens. The box lumens are included in the border resistance since the borders act as a bottleneck between the lumens and the pit.

$$R_{borders,t} = \frac{2\frac{\Delta x_a}{A_a} + 2\frac{\Delta x_c}{A_c} + 2\frac{\Delta x_l}{A_l}}{2\frac{\Delta x_a}{A_a} + 2\frac{\Delta x_c}{A_c} + \frac{\Delta x_m}{A_m} + 2\frac{\Delta x_l}{A_l}} \tag{27}$$

14

The border resistances in eq 11 and 27 are compared according to eq 28.

$$\frac{R_{borders}}{R_{borders,t}}$$ (28)

3.6.3 Membrane thickness and area

Varying the membrane thickness and area in eq 23 gives an indication of how sensitive the results are to a deviation from the used parameters. The total box length is kept same as in the base case (tab 6) as the membrane thickness is altered. To achieve this, the chamber length is adjusted.

4   Results

In this section the effective diffusion coefficients through a bordered pit for various sizes of dextran and enzymes are presented and the pit component's individual contribution to the total diffusive resistance is reported. Furthermore, the validity of the results was examined by using the theoretical model from section 3.5 and 3.6 and the information from the simulations with different resolutions (tab 4).

4.1   Effective diffusion coefficient

The simulation procedure described in section 3.3 resulted in effective diffusion coefficients 16.9 times smaller than the corresponding free diffusion coefficients. The effective diffusion coefficients of dextran and the enzymes is plotted against the molecular size in fig 10.
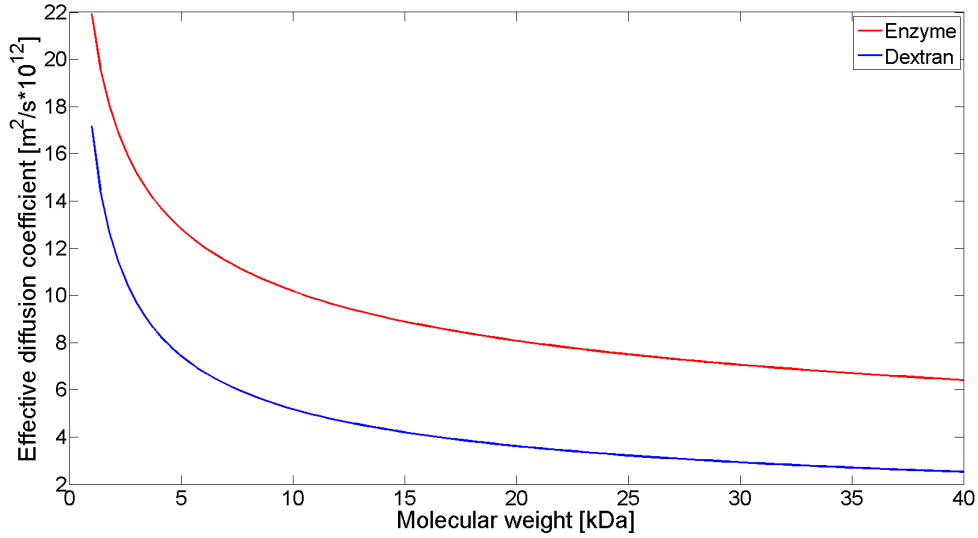

Figure 10: Effective diffusion coefficients of dextran and enzymes through a bordered pit.

The effective diffusion coefficient of dextran varies with the molecular weight as shown in eq 29.

$$D_{eff,dextran} = \frac{10^{1.2350}}{W^{13/25}} \tag{29}$$

where the unit of the effective diffusion coefficient is $\mu m^2/s$ and the molecular weight, W, is in kDa. The effective diffusion coefficient of the enzyme vary with the size as in eq 30.

$$D_{eff,enzyme} = \frac{10^{1.3412}}{W^{1/3}} \tag{30}$$

Equation 29 and 30 are valid for molecules sizes between 1 and 40 kDa.

4.2 Resistance to diffusion

By using eq 11, 12 and 13 the resistance of the individual pit components was determined to

- Borders: 98.8 %
- Torus: 1.1 %
- Margo: 0.1 %

Thus, the borders constitute most of the resistance to diffusion and the resistances imposed by the torus and margo are negligible in comparison.

4.3 Validation of results

This section presents the outcome of the validation of the simulation results, as delineated in section 3.6.

4.3.1 Effective diffusion coefficient

Equation 24 was used to compare the effective diffusion coefficient from the simulations with the theoretical diffusion coefficient in eq 23. The result is shown in eq 31.

$$\frac{D_{eff,t}}{D_{eff}} = 4.5 \tag{31}$$

The ratio in eq 31 is larger than 1 but smaller than 10 and therefore falls within the expected interval, as described in section 3.6.1.

4.3.2 Resistance to diffusion

The theoretical contribution of the borders and membrane to the total resistance to diffusion was computed using eq 25 and 27.

- Borders: 99.3 %
- Membrane: 0.7 %

The theoretical resistances was compared with the resistances in section 4.2 using eq 26 and 28, resulting in eq 32 and 33.

$$\frac{R_{borders}}{R_{borders,t}} = 99.5 \ \% \tag{32}$$

and

$$\frac{R_{membrane}}{R_{membrane,t}} = 167.6 \ \% \tag{33}$$

4.3.3 Membrane thickness and area

How the theoretical effective diffusion coefficient of a 10 kDa dextran polymer varies with the membrane thickness is shown in fig 11.
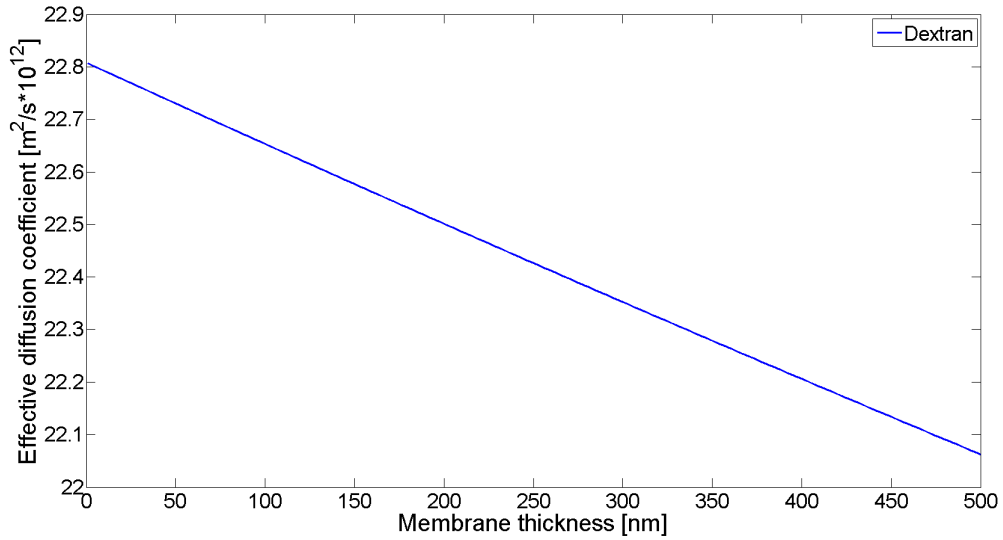
Figure 11: The effective diffusion coefficient of a 10 kDa dextran polymer at different membrane thicknesses.

Figure 11 indicates a 2.9 % decrease of the effective diffusion coefficient for an increase of the membrane thickness from 50 to 500 nm. A decrease of the membrane thickness from 50 to 25 nm increases the effective diffusion coefficient with 0.2 %.

At a membrane thickness of 500 nm the theoretical contribution of the borders and membrane to the total resistance to diffusion is 93.1 and 6.9 % respectively. At a thickness of 25 nm the corresponding values are 99.6 and 0.4 %.

Figure 12 shows the theoretical effective diffusion coefficient of dextran at various cross-sectional areas of the membrane.
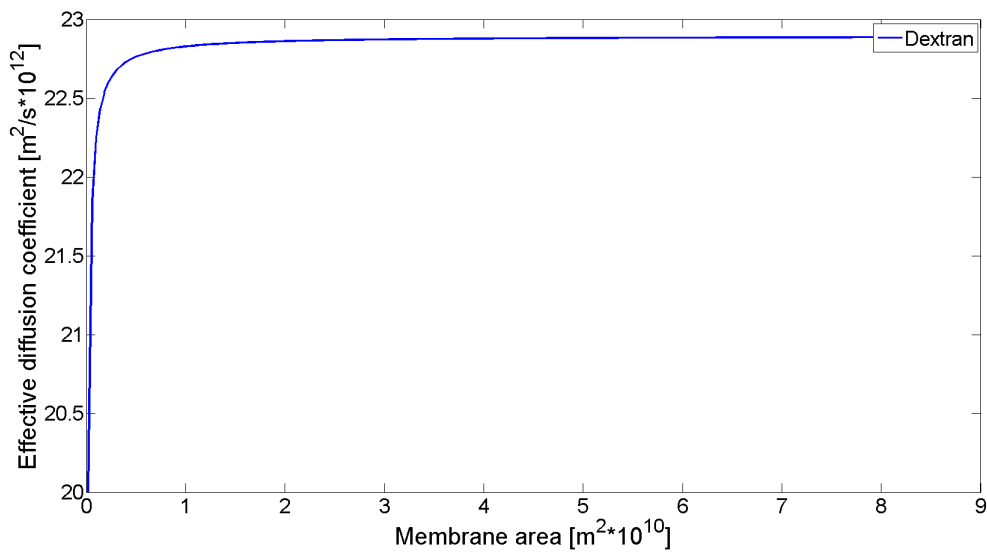

Figure 12: The effective diffusion coefficient of a 10 kDa dextran polymer at different membrane areas.

A twenty-fold increase of the cross-sectional membrane area from the used value (tab 7) results in a 0.7 % larger effective diffusion coefficient, and the membrane does not make up any resistance to diffusion at all. A twenty-fold decrease of the area reduces the effective diffusion coefficient with 12.0 %, but increases the contribution of the membrane to the total resistance to 12.6 %.

4.3.4 Grid dependence

Figure 13 shows the effective diffusion coefficient through pit model A (tab 1) for a 10 kDa dextran polymer at the six simulation resolutions specified in tab 4 and 5.
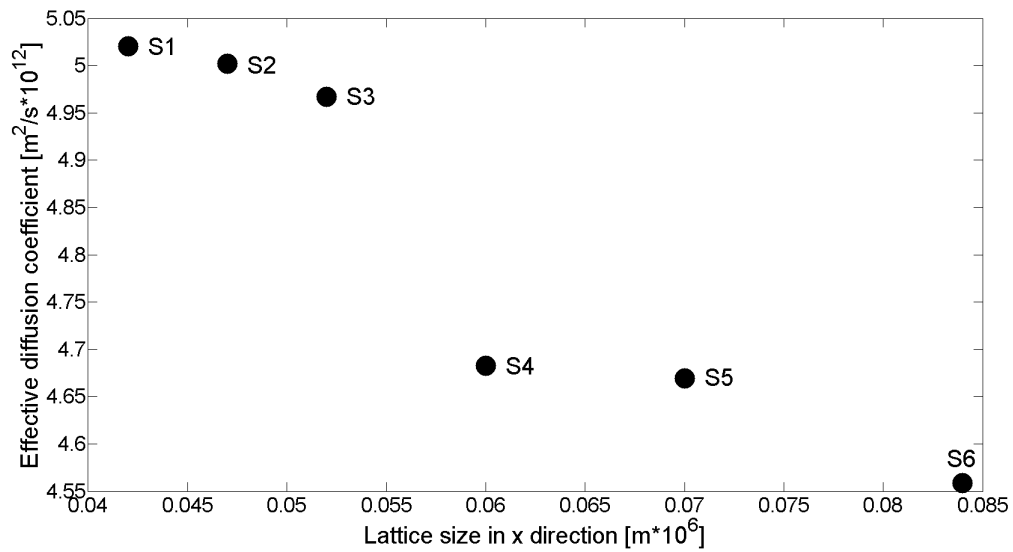

Figure 13: The effective diffusion coefficient of a 10 kDa dextran polymer at different resolutions (tab 4 and 5), through model A (tab 1).

A 10.6 % decrease of the resolution from S1 to S2 reduces the effective diffusion coefficient with 2.4 %. Reducing the resolution with 50 % (from S1 to S6) decreases the effective diffusion coefficient with 10.1 %.

5 Discussion

Values reported in the literature indicate that the pit structure varies depending on tree species and growth conditions, but variations are large even within the same tree. This suggests that the effective diffusion coefficients and diffusive resistances for a pit with different dimensions probably differ from those found in this work.

The pit dimensions are based on average values reported in the literature. The effective diffusion coefficients and resistances are therefore supposed to represent values relatively close to what would be obtained if an average for all earlywood pits in a conifer were calculated. However, an average of the membrane structure is difficult to determine. Varying the thickness and area of the membrane in the theoretical pit model (section 3.5 and 3.6) indicates that neither the thickness nor the area have any large impact on the results, unless the membrane is far thicker and denser than what have been reported in the literature.

An investigation of the grid dependence was carried out in section 4.3.4. It was found that the changes in the effective diffusion coefficient were small compared to the changes in resolution. Any large improvement of the results with increased resolution is therefore not likely. The sudden jump in effective diffusion coefficient between S3 and S4 in fig 13 is probably due to that the thin membrane is not sufficiently resolved in S4, S5 and S6.

It is not possible to verify the results with experimental data, due to the small size of pits. The order of magnitude of the effective diffusion coefficients was however confirmed by comparing them with those obtained from the theoretical model for diffusion through a pit. Furthermore, the pit component's individual resistances showed good agreement with the resistances from the theoretical model.

Schulte [8] modelled water flow through bordered pits and reported that the margo and torus together constitutes more than 80 % of the flow resistance. Valli et al [11] ascribed 38 % of the flow resistance to the margo. The membrane resistance for diffusion of large molecules was found to be 1 % in this work. The difference in resistances might partially be due to that the water was stagnant in the diffusion study. The frictional stresses on the torus and margo walls are zero in the diffusion case but non-zero in the flow case, resulting in a larger membrane resistance for the flow case.

By using the lattice Boltzmann method the diffusing molecules are modelled as rigid particles. Polymers and enzymes are not rigid, but were assumed not to entangle in each other or the margo pores, enabling the lattice Boltzmann approach. At a certain concentration and molecule size the polymers and enzymes cannot be modelled as rigid particles without accounting for the entanglement. To investigate such conditions was outside this work's scope.

6   Conclusions and future work

This work has determined effective diffusion coefficients of large molecules in a conifer earlywood bordered pit, as well as the pit component's individual contribution to the total resistance to diffusion. It was found that the effective diffusion coefficients are 16.9 times smaller than the free diffusion coefficients and that the borders constitutes 99 % of the resistance to diffusion. To increase the diffusive mass transfer rate through pits it is therefore necessary to partially or entirely remove the pit borders.

Even though dimensions varies from pit to pit, the border resistance is so much greater than the other resistances that it is unlikely that the margo or torus will impose the largest diffusive resistance if another pit was investigated. Future work could investigate this further by simulating diffusion through pits with a large variety of dimensions and margo structures.

References

[1] Causes of change [Internet]. Geneva: Intergovernmental Panel on Climate Change; 2007 [cited 2/1 2016]. Available from: https://www.ipcc.ch/publications_and_data/ar4/syr/en/spms2.html.

[2] M. FitzPatrick, P. Champagne, M. F. Cunningham, and R. A. Whitney. A biorefinery processing perspective: Treatment of lignocellulosic materials for the production of value-added products. *Bioresource Technology*, 101(23):8915 – 8922, 2010.

[3] S. Azhar, Y. Wang, M. Lawoko, G. Henriksson, and M. E. Lindström. Extraction of polymers from enzyme-treated softwood. *BioResources*, 6(4):4606–4614, 2011.

[4] Y. Zhang and L. Cai. Effects of steam explosion on wood appearance and structure of sub-alpine fir. *Wood Science and Technology*, 40(5):427–436, 2006.

[5] M. E. Himmel, S.-Y. Ding, D. K. Johnson, W. S. Adney, M. R. Nimlos, J. W. Brady, and T. D. Foust. Biomass recalcitrance: Engineering plants and enzymes for biofuels production. *Science*, 315(5813):804–807, 2007.

[6] J. F. Siau. *Transport processes in wood.* Springer Berlin Heidelberg, Berlin, Heidelberg, 2 edition, 1984.

[7] A. Wagner and L. Donaldson. *Applied plant cell biology: cellular tools and approaches for plant biotechnology*, chapter Metabolic engineering of wood formation, pages 369–391. Springer, New York; Heidelberg, 2014.

[8] P. J. Schulte. Computational fluid dynamics models of conifer bordered pits show how pit structure affect flow. *The New Phytologist*, 193(3):721–729, 2012.

[9] E. A. Behr, D. R. Briggs, and F. H. Kaufert. Diffusion of dissolved materials through wood. *Journal of Physical Chemistry*, 57(4):476–480, 1952.

[10] L. Wadsö. Bordered pit diffusion. Lund institute of technology, Division of building materials, 1988.

[11] A. Valli, A. Koponen, T. Vesala, and J. Timonen. Simulations of water flow through bordered pits of conifer xylem. *Journal of Statistical Physics*, 107(1):121–142, 2002.

[12] P. J. Schulte, U. G. Hacke, and A. L. Schoonmaker. Pit membrane structure is highly variable and accounts for a major resistance to water flow through tracheid pits in stems and roots of two boreal conifer species. *The New Phytologist*, 208(1):102–113, 2015.

[13] T. Song, A. Pranovich, and B. Holmbom. Separation of polymeric galactoglucomannans from hot-water extract of spruce wood. *Bioresource Technology*, 130:198–203, 2013.

[14] B. Butterfield. *Primary wood processing: principles and practice*, chapter The structure of wood: form and function, pages 1–22. Netherlands, Dordrecht, 2006.

[15] J.-C. Domec and B. Gartner. How do water transport and water storage differ in coniferous earlywood and latewood? *Journal of Experimental Botany*, 53(379):2369–2379, 2002.

[16] J. A. Petty. The aspiration of bordered pits in conifer wood. *Proceedings of the Royal Society of London B: Biological Sciences*, 181(1065):395–406, 1972.

[17] U. G. Hacke, J. S. Sperry, and J. Pittermann. Analysis of circular bordered pit function ii. gymnosperm tracheids with torus-margo pit membranes. *American Journal of Botany*, 91(3):386–400, 2004.

[18] A. L. Schoonmaker, U. G. Hacke, S. M. Landhäusser, V. J. Lieffers, and M. T. Tyree. Hydraulic acclimation to shading in boreal conifers of varying shade tolerance. *Plant, Cell & Environment*, 33(3):382–393, 2010.

[19] J.-C. Domec, B. Lachenbruch, and F. C. Meinzer. Bordered pit structure and function determine spatial patterns of air-seeding thresholds in xylem of Douglas-fir (pseudotsuga menziesii; pinaceae) trees. *American Journal of Botany*, 93(11):1588–1600, 2006.

[20] B. Choat, A. R. Cobb, and S. Jansen. Structure and function of bordered pits: new discoveries and impacts on whole-plant hydraulic function. *The New Phytologist*, 177(3):608–626, 2008.

[21] P. Trtik, J. Dual, D. Keunecke, D. Mannes, P. Niemz, P. Stähli, A. Kaestner, A. Groso, and M. Stampanoni. 3D imaging of microstructure of spruce wood. *Journal of Structural Biology*, 159(1):45–55, 2007.

[22] J. C. F. Walker. *Primary wood processing: principles and practice*, chapter Basic wood chemistry and cell wall ultrastructure, pages 23–67. Springer, Netherlands, Dordrecht, 2006.

[23] H. Ylmaz Celebioglu, D. Cekmecelioglu, M. Dervisoglu, and T. Kahyaoglu. Effect of extraction conditions on hemicellulose yields and optimisation for industrial processes. *International Journal of Food Science & Technology*, 47(12):2597–2605, 2012.

[24] J. Crank. *The mathematics of diffusion*. Clarendon Press, Oxford, 2. edition, 1979.

[25] E. L. Cussler. *Diffusion: mass transfer in fluid systems*. Cambridge University Press, Cambridge, 3. edition, 2009.

[26] J. R. Welty, C. E. Wicks, R. E. Wilson, and G. L Rorrer. *Fundamentals of momentum, heat, and mass transfer*. Wiley, Chichester; Hoboken, N.J;, 5 edition, 2008.

[27] H. Erickson. Size and shape of protein molecules at the nanometer level determined by sedimentation, gel filtration, and electron microscopy. *Biological Procedures Online*, 11(1):32–51, 2009.

[28] L. Shen and Z. Chen. Critical review of the impact of tortuosity on diffusion. *Chemical Engineering Science*, 62(14):3748–3755, 2007.

[29] A. A. Mohamad. *Lattice Boltzmann method: fundamentals and engineering applications with computer codes.* Springer, New York; London, 2011.

[30] M. C. Sukop and D. T. Thorne. *Lattice Boltzmann modeling: an introduction for geoscientists and engineers.* Springer, New York; Berlin, 1 edition, 2006.

[31] P. L. Bhatnagar, E. P. Gross, and M. Krook. A model for collision processes in gases. I. Small amplitude processes in charged and neutral one-component systems. *Physical Review*, 94(3):511–525, 1954.

[32] I. Ginzburg. Equilibrium-type and link-type lattice Boltzmann models for generic advection and anisotropic-dispersion equation. *Advances in Water Resources*, 28(11):1171–1195, 2005.

[33] A. Zarghami, S. Ubertini, and S. Succi. Finite-volume lattice boltzmann modeling of thermal transport in nanofluids. *Computers and Fluids*, 77:56–65, 2013.

[34] J. G. Zhou. *Lattice Boltzmann methods for shallow water flows.* Springer, Berlin, Heidelberg, 2004.

[35] T. Gebäck and A. Heintz. A lattice Boltzmann method for the advection-diffusion equation with Neumann boundary conditions. *Communications in Computational Physics*, 15(2):487–505, 2014.

[36] S. Chen and G. D. Doolen. Lattice Boltzmann method for fluid flow. *Annual review of fluid mechanics*, 30(1):329–364, 1998.

[37] J. Bernsdorf. *Simulation of complex flows and multi-physics with the lattice-Boltzmann method.* PhD thesis, University of Amsterdam, 1 2008.

[38] M. Arrio-Dupont, S. Cribier, G. Foucault, P. Devaux, and A. d'Albis. Diffusion of fluorescently labeled macromolecules in cultured muscle cells. *Biophysical Journal*, 70(5):2327–2332, 1996.